Applied Acoustics 255 (2027) 111502

Contents lists available at ScienceDirect

Applied Acoustics

journal homepage: www.elsevier.com/locate/apacoust

Impact of electric mobility on urban noise levels predicted by time-resolved noise maps

Tobias S. Müller[a,*], Daniel Krajzewicz[b], Arne Henning[a]

[a] German Aerospace Center (DLR), Bunsenstr. 10, Göttingen, 37073, Germany
[b] German Aerospace Center (DLR), Rutherfordstr. 2, Berlin, 12489, Germany

HIGHLIGHTS

- Impact of the transition from ICEVs to EVs on traffic noise is explored.
- Time-resolved noise-mapping technique with high resolution is applied.
- Two EV noise emission models are applied and compared.
- Impact on wake-up risk is quantified using an exposure-response relationship.

ARTICLE INFO

Keywords:
Electric mobility
Traffic noise
Noise-mapping techniques

ABSTRACT

The transition from internal combustion engine vehicles (ICEVs) to electric vehicles (EVs) is a key component of urban decarbonization, yet its acoustic implications remain not fully captured by conventional noise assessment. This study presents a time-resolved noise mapping framework which is based on the CNOSSOS-EU guideline and driven by a microscopic traffic simulation, enabling the detailed analysis of transient noise events. The method is applied to the district of Gross Flottbek in Hamburg, Germany, to assess the impact of fleet electrification on noise pollution and human health. To model EV noise emissions, two recently proposed modifications of the CNOSSOS-EU emission model are implemented and compared. Besides the equivalent continuous night-time sound level L_{Night}, the impact on wake-up reactions triggered by isolated pass-by events is studied. The results indicate that the overall impact on sleep quality from the transition to EVs remains moderate. The greatest impact on wake-up reactions is found along major and intermediate-traffic roads, while reductions of L_{Night} are most pronounced in quieter residential areas. These findings demonstrate that time-resolved noise mapping is a valuable tool for a comprehensive evaluation of noise exposure, as it reveals health-relevant insights, such as the acute impact of transient events, which conventional average-based methods tend to miss.

1. Introduction

Urban noise pollution, primarily driven by road traffic, constitutes a significant public health concern, contributing to sleep disruption, cardiovascular stress, and reduced quality of life [1–7]. The World Health Organization (WHO) estimates that at least one million healthy disability-adjusted life years are lost every year due to the impact of environmental noise [8]. As cities worldwide pursue decarbonization strategies, the transition from internal combustion engine vehicles (ICEVs) to electric vehicles (EVs) is gaining momentum. This transition is expected not only to significantly reduce greenhouse gas emissions and local air pollutants but also to reshape urban acoustic environments through a substantial decrease in road-traffic noise pollution especially at low speeds. The extent to which the transition from ICEVs to EVs will reduce traffic noise pollution remains, however, a subject of ongoing debate, underscoring the need for reliable simulation and modeling techniques capable to assess the acoustic implications of fleet electrification.

In this context, numerical noise-mapping techniques represent a powerful and indispensable tool for evaluating changes in traffic-related noise pollution resulting from shifts in vehicle fleets or from the implementation of traffic management policies. The importance of such tools is further underscored by the European Union's Environmental Noise Directive (2002/49/EC) [9], which requires member states to produce strategic noise maps every five years for urban areas with populations

* Corresponding author.
Email address: tobias.mueller@dlr.de (T.S. Müller).

https://doi.org/10.1016/j.apacoust.2026.111502
Received 2 March 2026; Received in revised form 10 July 2026; Accepted 31 July 2026
Available online 14 August 2026

exceeding 100,000 inhabitants. These maps are used to assess exposure to road, rail, and aircraft noise and to inform the development of noise action plans. To ensure methodological consistency and cross-city comparability, the directive mandates the use of the CNOSSOS-EU framework [10], a harmonized approach for noise prediction that enables reliable assessment of long-term average noise levels across Europe. Consequently, the development and application of accurate, scalable, and computationally efficient noise-mapping methodologies is not only scientifically valuable but also essential for compliance with regulatory frameworks and for supporting evidence-based decision-making in sustainable urban development.

Noise mapping techniques based on acoustic exposure metrics derived from time-averaged energetic doses, such as the day-evening-night noise level L_{den} or the equivalent continuous sound level L_{eq} for one or several hours, have long served as the cornerstone of environmental noise assessment, enabling consistent evaluation of traffic noise exposure [11–14] and its impact on human health and well-being [7,15–19]. These metrics are widely used in urban planning, policy-making, and regulatory frameworks and have successfully informed mitigation strategies, particularly in identifying areas exceeding recommended exposure thresholds [12,14].

The basis of any noise mapping technique targeting urban environments is the traffic-flow modeling, which can be broadly categorized into three levels: static, mesoscopic and microscopic. Static models rely on average traffic data and assume a free flow of uniformly distributed vehicles driving at constant speed. While suitable for computing energy-based indicators such as L_{eq} [12,20–22], they fail to capture dynamic variations in traffic noise. Mesoscopic models assume that all vehicles are independent from one another but account for the distribution of mean speeds across the road network. In contrast, microscopic models simulate individual vehicle interactions and are thus capable to deliver dynamic phenomena, such as acceleration, deceleration, and congestion at intersections. These dynamics have a substantial impact on noise levels and prediction models based on microscopic traffic simulation have been found to outperform the other two approaches [23]. However, due to their high computational cost, many studies rely on mesoscopic simulation frameworks such as MATSim to assess the impact of traffic noise on the population [13,24,25]. As computational capabilities continue to advance, microscopic simulation models are gaining increasing popularity for high-fidelity urban noise assessment [14,26–29]. These models are able to capture subtle temporal features in traffic noise, such as the sharp rise and decay caused by pass-by events, which are inaccessible by static or mesoscopic methods.

The temporal structure of traffic noise, particularly the characteristics of transient events, plays a crucial role in determining annoyance and physiological responses. Studies on sleep disturbance have shown that isolated noise events, such as single vehicle pass-bys, carry a high probability of inducing wake-up reactions [4,30–34]. The likelihood of awakening is not primarily governed by long-term averages (such as L_{eq} or L_{den}) but rather by the peak characteristics of the noise events. In particular, the maximum sound pressure level L_{max} during a pass-by has been identified as a key predictor of sleep disturbances [5,30,31,34], with higher L_{max} values significantly increasing the risk of inducing wake-up reactions. While other temporal features, such as the rise time or slope of the noise signal, also contribute [32], L_{max} remains one of the most robust metrics for assessing the acute impact of individual traffic events on sleep quality. This underscores the need for noise assessment methods that resolve the temporal microstructure of traffic noise with sufficient fidelity to capture these critical transient phenomena.

The need for such noise-assessment methods is particularly pressing in the context of emerging urban mobility paradigms, such as the aforementioned transition from ICEVs to EVs. However, to date only a limited number of studies have employed noise-mapping techniques to investigate the impact of this transition [11,14], which might be partially related to the fact that explicit emission coefficients for EVs are still missing in noise-assessment frameworks such as CNOSSOS-EU.

The present study aims to fill this gap by providing an insight to the transition from ICEVs to EVs from a time-resolved noise-mapping perspective. The method is based on the CNOSSOS-EU framework, and the two recently proposed models by Pallas et al. [35] and Licitra et al. [36] for simulating EV noise emissions are applied and compared. The time-resolved microscopic nature of the method can be expected to enable a more realistic assessment of the impact of EVs than static or mesoscopic approaches.

Furthermore, the method enables the detection of isolated noise events at representative observer locations during nighttime and to extract the corresponding maximum sound pressure level L_{max}. These peak levels are employed to estimate the probability of induced wake-up reactions by means of the exposure-response relation proposed by Sanok et al. [34]. This allows to quantify the effect on sleep disturbance caused by fleet electrification, and to compare these findings with those obtained using standard metrics, such as the equivalent continuous night-time sound level L_{Night}.

2. Generating time-resolved noise maps

To assess the urban road-traffic noise pollution and its effects on the population, we generate high-resolution, time-resolved noise maps covering an entire district in the city of Hamburg, Germany. The maps are based on a microscopic traffic simulation covering the area and are computed using an adaptation of the CNOSSOS-EU framework [10]. The microscopic traffic simulation as well as the three-step process to generate the time-resolved noise maps are described in more detail in the following.

2.1. Microscopic traffic simulation

The generation of time-resolved noise maps is driven by SUMO (Simulation of Urban Mobility) [37]. SUMO is an open-source, microscopic traffic simulation platform widely used for modeling urban traffic at the level of individual vehicles. In the present work SUMO is applied to simulate the traffic flow on a detailed representation of the road network in a district of Hamburg.

The traffic demand used as input to SUMO is generated using TAPAS (Travel and Activity Patterns Simulation) [38]. Given a synthetic, disaggregated population, activity places within the modeled area, and performance indicators of the modeled transport systems, TAPAS generates daily activity plans for each person in the population, including the departure time, the start and end positions of each trip, as well as the mode of transport. TAPAS relies on empirical data of about 50,000 daily plans to cover all performed activities—including home, work, shopping, and leisure activities—and their combinations. This agent-based approach ensures that traffic demand is not only temporally and spatially realistic but also reflects the underlying socio-demographic and behavioral patterns of the population. TAPAS results are validated against trip length distributions and the area's modal split.

In the present work, only trips performed by car are considered and provided as input to SUMO. Given the departure time, the origin and destination of the trips for all vehicles in the area, SUMO is first used to compute the assignment-route choice in a loaded network, then to simulate the vehicles' progress through the road network. The simulated vehicles regard the given infrastructure, including traffic lights, right-of-way-rules, etc. and interact with each other using so-called car-following models. On a macroscopic scale, the traffic flow, i.e., the number of vehicles passing a road section over time, is validated using the city's traffic counter data. On a microscopic scale, prior work showed a sufficient match between the simulated vehicles' dynamics and the corresponding real-world values, as reported by Schrader et al. [39]. The present work uses the standard SUMO parameters for vehicles and the simulated vehicle trajectories serve as the primary input for the noise-mapping process, allowing for a dynamic and population-representative assessment of the road-traffic noise sources.

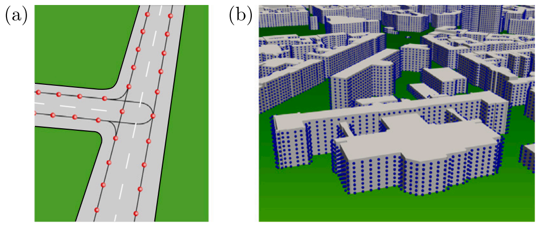

Fig. 1. (a) Static emitter points positioned at regular intervals along each lane of the road network. (b) Static receiver points positioned at a fixed distance in front of building façades. Note that, for visual clarity, the figure shows a grid of façade receivers, while the applications in Section 4.2 are based on data from a single façade receiver per building.

2.2. Geometry processing

As a preliminary step in generating the time-resolved noise maps, the geometric features of the study area are modeled, which include the road network and surrounding buildings. Terrain elevation is neglected since the study area is predominantly flat, with a maximum difference in elevation of about 16 m across the entire domain. Furthermore, vegetation is not included in the model. This simplification is justified in urban environments, where the influence of vegetation on noise propagation is typically secondary to that of buildings and walls.

The road network is sourced from OpenStreetMap [40] data and serves as an input to the microscopic traffic simulation SUMO. Building geometries are represented at Level of Detail 1 (LoD1), where each structure is modeled as a polygonal footprint extruded to its corresponding height, providing a simplified yet sufficiently accurate representation of urban morphology. Following the geometric setup of the buildings, static emitter points are placed along the individual lanes of the road network at regular intervals of 2 m to represent potential vehicle positions, as illustrated in Fig. 1(a). Furthermore, static receiver points are distributed on a regular grid 1.5 m above the ground and 2 m in front of the façades of selected buildings (see Fig. 1b) to capture the noise exposure at relevant observer locations. These static points serve as proxies for vehicle locations and potential human observers, respectively.

The choice of *static* emitter locations allows for the precomputation of the acoustic propagation paths between all relevant emitter-receiver pairs, which significantly reduces the computational costs for generating time-resolved noise maps covering extended periods of time (e.g., multiple hours or days), as the propagation paths do not need to be calculated at each time step for every moving vehicle. Moreover, the use of static emitter points allows for the straightforward evaluation of multiple traffic scenarios on the same urban geometry, as the acoustic propagation paths remain unchanged and do not require recomputation, thereby facilitating rapid comparative assessments of different traffic configurations, emission profiles (e.g., ICEVs versus EVs), or policy interventions.

2.3. Ray tracing

To determine the dominant sound propagation paths between emitter-receiver pairs, homogeneous conditions are assumed (i.e., sound is assumed to propagate along straight line segments) and a ray-tracing technique which incorporates both reflections on building façades and diffraction on horizontal and vertical building edges is employed. Specifically, the ray-tracing method accounts for the four ray types defined in the CNOSSOS-EU guideline [10]:

- Type 1: Allows diffraction on horizontal (roof-top) edges,
- Type 2: Allows reflections on building façades as well as diffraction on horizontal (roof-top) edges,
- Type 3: Allows diffraction on vertical building edges,
- Type 4: Allows reflections on building façades as well as diffraction on vertical edges.

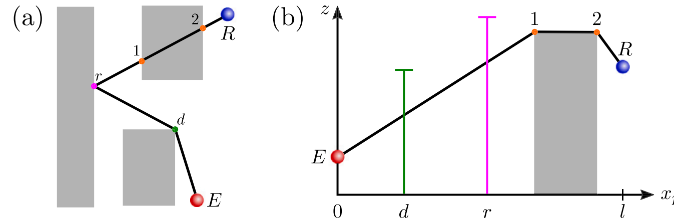

Fig. 2. (a) Top-down view of an acoustic propagation path connecting an emitter E to a receiver R in a simplified urban environment (rectangles represent buildings). The path contains a diffraction d at a vertical building edge, a reflection r on a building façade and intersects building edges at points 1 and 2. (b) Ray profile in the vertical scheme obtained by "unfolding" the ray at the reflection and diffraction points. Reflection and diffraction locations are marked by vertical lines extending to the height of the corresponding building. Points 1 and 2 correspond to the locations where the ray intersects building edges in the top-down view and are drawn at the height of the corresponding building.

The construction of the rays is based on the 2.5D method specified in the CNOSSOS-EU guideline [10]. It relies on the fact that buildings are represented at LoD1, which enables the identification of reflective façades and diffracting edges in a top-down view of the urban scene. The construction of the rays in the 2D top-down view is similar to the image-source method [41,42], used to compute all possible reflection paths that connect a source to any receiver in its vicinity. However, the present method treats building corners visible from the source as secondary sources to model diffraction on vertical building edges. Here, secondary sources are considered only for corners exhibiting a shadow region when seen from the source's point of view, in order to focus on diffractions into shadow regions. Direct rays are dominant in the light region such that the acoustical contribution of diffracted rays is rather negligible. Fig. 2(a) shows a schematic example of an acoustic propagation path in the top-down view of a simplified urban environment. The ray is emitted by the source labeled E, incorporates a diffraction (d) on a vertical building edge into the shadow region and a subsequent reflection (r) on a building façade before it arrives at a receiver labeled R. The ray is allowed to intersect building edges (points 1 and 2) in the top-down view, since these intersections are candidates for diffraction at horizontal roof edges.

In order to construct the ray profile, one constructs a vertical scheme where the coordinate x_p on the horizontal axis represents the path length along the ray in the top-down view (see Fig. 2b). Emitter E and receiver R are marked at $(0, z_E)$ and (l, z_R) respectively, where z_E and z_R refer to the height of emitter and receiver, respectively, and l to the total length of the ray in the top down view. Furthermore, the locations where the ray intersects building edges in the top-down view are marked at the corresponding x_p coordinate at the height z of the intersected building (points 1 and 2 in Fig. 2b). The ray profile is then obtained as the upper convex hull of the emitter E, receiver R and the intersection points. The final step is to verify that the ray profile is consistent with the reflections and diffractions. To this aim, vertical lines are constructed at the path-length coordinate x_p of the reflection and diffraction points, extending to the height of the building on which the ray is reflected or diffracted (see vertical lines marked d and r in Fig. 2b). If the ray profile intersects all of these vertical lines the ray profile is valid and a final 3D ray is readily obtained; otherwise the ray is invalid and must be discarded.

Notice that the ray constructed in Fig. 2 does not fall into any of the four categories defined above, since it incorporates diffractions on *both* vertical and horizontal building edges, i.e., the method described is able to produce more complex rays than required by the CNOSSOS-EU guideline. For consistency with the CNOSSOS-EU guideline and to reduce computational complexity, rays involving mixed-type diffractions are excluded in the framework of the present study. Furthermore, to ensure convergence of the ray-tracing algorithm and to focus on

Table 1
Emission coefficients for light ICEVs ($m = 1$ category) and EVs employed in the framework of the present study. The coefficients for ICEVs are taken from the German BUB directive [43], while the coefficients for EVs are taken from the two emission models proposed by Pallas et al. [35] and Licitra et al. [36].

	A_R			B_R			A_P			B_P		
Freq. [Hz]	ICEVs	Pallas	Licitra	ICEVs	Pallas	Licitra	ICEVs	Pallas	Licitra	ICEVs	Pallas	Licitra
63	83.1	79.7	88.1	30.0	30.0	24.7	97.9	94.5	0.0	−1.3	−1.3	0.0
125	89.2	85.7	86.5	41.5	41.5	23.4	92.5	87.5	0.0	7.2	7.2	0.0
250	87.7	84.5	89.3	38.9	38.9	17.5	90.7	83.8	0.0	7.7	7.7	0.0
500	93.1	90.2	92.3	25.7	25.7	30.8	87.2	70.9	0.0	8.0	8.0	0.0
1000	100.1	97.3	96.0	32.5	32.5	39.3	84.7	69.2	0.0	8.0	8.0	0.0
2000	96.7	93.9	92.8	37.2	37.2	41.2	88.0	71.9	0.0	8.0	8.0	0.0
4000	86.8	84.1	83.3	39.0	39.0	39.9	84.4	69.5	0.0	8.0	8.0	0.0
8000	76.2	74.3	71.9	40.0	40.0	31.2	77.1	76.1	0.0	8.0	8.0	0.0

acoustically significant propagation paths, constraints must be imposed on the number of reflections, diffractions, and the total path length. In this study, rays are limited to involve a maximum of two reflections on building façades and one diffraction at vertical building edges. Additionally, receivers located beyond 600 m from the source are neglected, and rays with a total path length exceeding 750 m are discarded. These thresholds balance computational efficiency with physical relevance, ensuring that only the most impactful sound propagation paths are considered.

The final step in the ray-tracing process involves computing the attenuation A_i of sound traveling along the rays for the eight octave bands ranging from 63 Hz to 8 kHz, which is done by using the attenuation rules specified in the CNOSSOS-EU guideline [10, Sec. VI.4].

2.4. Noise emission and propagation

The last step is to compute the time-resolved sound pressure level (SPL) at the individual receiver sites in order to obtain the final noise map. To this aim, the individual vehicle trajectories obtained from the microscopic traffic simulation SUMO [37] (see Section 2.1) are sampled at a temporal resolution of 1/8 s, which yields the vehicle type (passenger car, delivery van, bus, truck, etc.), its location, speed and acceleration at each time step.

According to the CNOSSOS-EU guideline [10, Sec. III.2], the sound-power level (SWL)

$$L_{W,i,m} = 10\,\log_{10}\left(10^{L_{W\,R,i,m}/10} + 10^{L_{W\,P,i,m}/10}\right) \tag{1}$$

emitted in the octave band i by a single vehicle belonging to category m is obtained as the energetic sum of the rolling noise $L_{W\,R,i,m}$ and the propulsion noise $L_{W\,P,i,m}$. The four considered vehicle categories are [10]:

1. Light motor vehicles (passenger cars, delivery vans ≤ 3.5 t, Sport Utility Vehicles, Multi-Purpose Vehicles including trailers and caravans)
2. Medium heavy vehicles (medium heavy vehicles, delivery vans > 3.5 t, buses, touring cars, etc. with two axles and twin tyre mounting on rear axle)
3. Heavy vehicles (heavy duty vehicles, touring cars, buses, with three or more axles)
4. Powered two-wheelers (4a: mopeds, tricycles or quads ≤ 50 cc; 4b: motorcycles, tricycles or quads > 50 cc).

Reference conditions are assumed, i.e., a flat road, an air temperature of 20 °C and a dry road surface consisting of dense asphalt concrete 0/11 and stone mastic asphalt 0/11, between 2 and 7 years old and in a representative maintenance condition. Under these conditions, the rolling and propulsion noise emission is given by

$$L_{W\,R,i,m} = A_{R,i,m} + B_{R,i,m}\,\log_{10}\left(\frac{v}{v_{\mathrm{ref}}}\right) + \Delta L_{W\,R,\mathrm{acc},i,m} \tag{2}$$

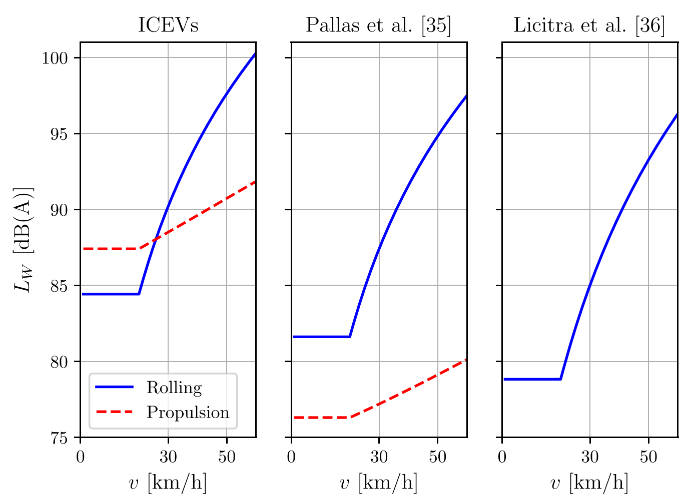

Fig. 3. A-weighted rolling- and propulsion-noise components of the emitted sound-power level as functions of vehicle speed v for light ICEVs ($m = 1$ category) and EVs using the Pallas et al. [35] and Licitra et al. [36] models.

$$L_{W\,P,i,m} = A_{P,i,m} + B_{P,i,m}\,\frac{v - v_{\mathrm{ref}}}{v_{\mathrm{ref}}} + \Delta L_{W\,P,\mathrm{acc},i,m}\,, \tag{3}$$

where v is the vehicle's momentary velocity in km/h and $v_{\mathrm{ref}} = 70$ km/h is the reference speed. For velocities below 20 km/h the emissions obtained from Eqs. (2) and (3) for $v = 20$ km/h are used. The explicit values of the coefficients $A_{R,i,m}$, $B_{R,i,m}$, $A_{P,i,m}$ and $B_{P,i,m}$ employed in the present work for light ICEVs ($m = 1$ category) and EVs are listed in Table 1 and the resulting speed dependence of the A-weighted rolling and propulsion-noise components is shown in Fig. 3. For all ICEVs (categories 1–4) the coefficients specified in the German BUB directive [43] are used, as they are believed to allow for a slightly more accurate representation of the German vehicle fleet than the values provided in the CNOSSOS-EU guideline.[1] For light EVs the emission coefficients proposed by two distinct models are employed: Pallas et al. [35] and Licitra et al. [36]. A short review and comparison of these models is provided in Section 3.

Leveraging the fact that the microscopic traffic simulation provides the vehicle's acceleration a at each time step, we employ in Eqs. (2) and (3) a semi-custom correction for the contribution of the acceleration noise:

$$\Delta L_{W\,R,\mathrm{acc},i,m} = C_{R,m}\,\min\left\{1,\,\max\left\{0,\,a/(3\,\mathrm{m/s^2})\right\}\right\} \tag{4}$$

[1] The road-traffic noise emission model defined in the German BUB directive is largely consistent with that of the amended version of the EU Directive 2002/49/EC from 2021 [44].

$$\Delta L_{WP,\mathrm{acc},i,m} = C_{P,m}\,\min\Big\{1,\,\max\big\{0,\,a/(3\,\mathrm{m/s^2})\big\}\Big\}, \tag{5}$$

where $C_{R,m}$ and $C_{P,m}$ are the acceleration-noise coefficients for a road crossing ($k = 1$) specified in the German BUB directive [43]. This choice ensures that the acceleration noise never exceeds the bounds implied by the BUB directive. Note that Eqs. (4) and (5) account for acceleration noise only, i.e., there is no contribution from decelerating vehicles. The correction increases linearly with positive acceleration until the maximum value is reached for $a = 3\,\mathrm{m/s^2}$, which is a reasonable upper bound for accelerations observed in typical traffic situations. In the following applications (Section 4) this semi-custom correction for the contribution of the acceleration noise is applied to both, ICEVs and EVs. In the case of EVs, this might lead to a slight overestimation of the acceleration noise, but since the two EV emission models proposed by Pallas et al. [35] and Licitra et al. [36] do not incorporate explicit modifications to the acceleration noise component, we treat ICEVs and EVs on the same footing. Notice, however, that a recent contribution by Baclet et al. [45] proposes a dedicated correction model for the acceleration noise of EVs, which presents a promising basis for future improvements in modeling EV noise emissions.

Independent of its actual size, each vehicle is regarded as a single point source located 0.05 m above the road surface, emitting a SWL $L_{W,i,m}$ obtained from Eq. (1). However, the instantaneous position of a given vehicle at a given time step typically does not coincide with one of the fixed emitter points placed along the lanes of the road network. Thus, to approximate the vehicle's momentary position, the two closest emitters on its driving lane are selected. These two emitters encompass the vehicle's location: one emitter is in front and the other behind it. The emitted sound power, $W_{i,m} = W_0\,10^{L_{W,i,m}/10}$ with reference sound power $W_0 = 1\,\mathrm{pW}$, is then distributed between these two emitters according to

$$W_{E,i,m} = W_{i,m}\left(1 - \frac{s_E}{s_1 + s_2}\right), \tag{6}$$

where s_E is the distance between emitter $E = 1, 2$ and the vehicle's actual location. Notice that this distribution of the emitted sound power between the two emitters encompassing the vehicle's position is not the result of modeling the vehicle's emission by multiple sources, but rather an interpolation of the vehicle's location onto the fixed emitter grid.

Lastly, the sound power is propagated from the emitters to the receivers along the precomputed rays: Assume that emitter E emits a sound power $W_{E,i,m}(t)$ at a given time t and that E is connected to receiver R via a ray of total length l. One then adds the contribution

$$\Delta p_{R,i}^2(t + l/c) = p_0^2\,\frac{W_{E,i,m}(t)}{W_0}\,10^{-A_i/10} \tag{7}$$

to the squared sound pressure at the receiver site for the advanced time $t + l/c$, where c is the speed of sound, $A_i > 0$ is the attenuation of sound within the frequency band i propagating along the ray, and $p_0 = 20\,\mu\mathrm{Pa}$ is the reference pressure. Once all contributions to the squared sound pressure at the receiver site have been accumulated for a given time t, the final value of the momentary SPL is obtained as $L_R(t) = 10\log_{10}\big[\sum_i 10^{\alpha_i/10}\,p_{R,i}^2(t)/p_0^2\big]$, where α_i is the A-weighting correction for the frequency band i.

3. EV emission models

The present work focuses on the two emission models for light EVs proposed by Pallas et al. [35] and Licitra et al. [36]. In the following we provide a brief overview of these two models, focusing on the aspects most relevant in the framework of the present study.

3.1. Pallas et al. model

As a first step towards extending the CNOSSOS-EU [10] framework to light EVs, Pallas et al. [35] performed experimental measurements on a sample of vehicles to derive suitable values for the emission coefficients $A_{R,i,m}$, $B_{R,i,m}$, $A_{P,i,m}$ and $B_{P,i,m}$ defined in Eqs. (2) and (3). Their finding is that the CNOSSOS-EU emission model for light motor vehicles ($m = 1$ category) overestimates the noise levels of EVs in most octave bands at low and medium speeds (up to 50–60 km/h). This overestimation has been found to be mostly due to the propulsion noise component. The use of tires targeted for EVs did not show any significant effect on the rolling noise; thus Pallas et al. decided to propose a modification of the CNOSSOS-EU coefficients for the propulsion noise only. Their modification has the form of constant correction coefficients $\Delta L_{WP,\mathrm{EV},i}$ for the octave bands i with center frequencies ranging from 125 Hz to 4 kHz. These constant correction terms can be absorbed into the coefficients $A_{P,i,m}$ defined in Eq. (3). The resulting emission coefficients for EVs in the framework of the Pallas et al. model are listed in Table 1 and the corresponding dependence of the rolling- and propulsion-noise components on the vehicle speed v is shown in Fig. 3.

3.2. Licitra et al. model

Several years after the study of Pallas et al. a new set of measurements was performed by Licitra et al., aiming to derive CNOSSOS-EU emission coefficients for light EVs. Their work is based on a versatile fleet of EVs: Nissan Leaf, Hyundai Ioniq, Nissan NV200 and Tesla Model 3. The maximum sound level was determined in controlled pass-by measurements on a test road located in Florence, Italy, consisting partly of crumb rubber pavement (CRP) and partly of reference pavement (RP). Also the impact of different sets of tyres was investigated in the framework of their study. In contrast to the model of Pallas et al., Licitra et al. consider the propulsion noise of EVs as negligible and emission coefficients are derived for the rolling-noise component only. The present work employs the coefficients derived by Licitra et al. for RP, which are listed in Table 1. These coefficients result in the speed dependence of the rolling-noise component displayed in Fig. 3. For the case of CRP, Licitra et al. derived a set of correction coefficients which are not used in the present work. Some comments on the work of Licitra et al. and a corrected figure have been provided by Pallas [46].

4. Predicting the impact of electric mobility

To assess the impact of transitioning from ICEVs to a fleet dominated by EVs on road-traffic noise in urban areas, we focus on the district of Gross Flottbek in Hamburg-Altona, Germany (see Fig. 4). Spanning approximately $2.0 \times 1.7\,\mathrm{km}^2$ with a population of around 11,000 residents, this area offers a representative mix of traffic conditions: quieter residential streets alongside high-traffic arterial roads. This diversity makes it well-suited to capture the range of noise scenarios commonly encountered in urban environments across Europe, enabling a robust evaluation of the acoustic effects of fleet electrification within different traffic contexts.

Around 50,000 static emission points are placed along the lanes of the road network at 0.05 m height, as required by the CNOSSOS-EU guideline. Over 100,000 receivers are arranged in a regular grid covering the whole domain (excluding building interiors) with 5 m cell width along the x- and y-directions and a height of 1.5 m. Additional receivers are positioned in front of the façades of selected buildings to capture noise exposure at critical urban receptor points.

Time-resolved noise maps are generated as described in Section 2, covering a full 24-hour period with a temporal resolution of 1/8 s, enabling the detailed characterization of transient traffic noise events, such as individual vehicle pass-bys, including their onset, peak, and decay characteristics. In the following sections, we focus on the nighttime period from 11 p.m. to 7 a.m., when traffic noise exposure poses the greatest risk to human health. During sleep, individuals are particularly vulnerable to noise disturbances, and especially brief, high-peak events, such as individual vehicle pass-bys, can induce wake-up reactions and disrupt sleep quality [4,30–34]. Long-term exposure to nighttime traffic noise has been consistently linked to a range of adverse health effects,

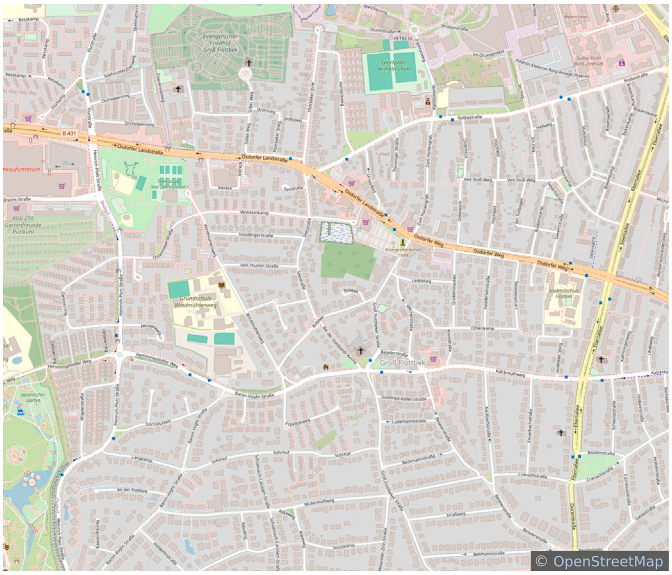

Fig. 4. Study area: Gross Flottbek in Hamburg-Altona, Germany. The $2.0 \times 1.7\,\mathrm{km}^2$ district features a representative mix of residential and high-traffic roads, enabling the assessment of noise exposure under different traffic scenarios during the transition from ICEVs to EVs. Figure taken from OpenStreetMap (©OpenStreetMap contributors [40]).

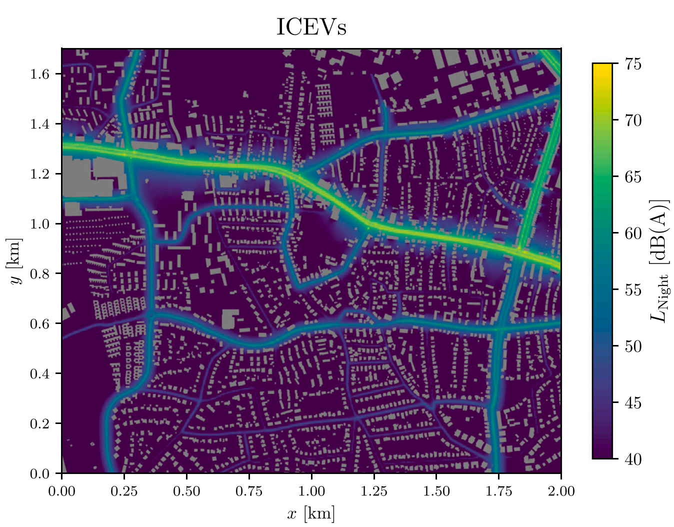

Fig. 5. Equivalent continuous sound pressure level L_{Night} during the nighttime (11 p.m. to 7 a.m.) derived from time resolved noise maps for the case of a conventional fleet of ICEVs. The color map accounts for values ranging from 40 to 75 dB(A), as indicated by the color bar on the right, and grey polygons represent buildings within the domain.

including increased risk of cardiovascular diseases, hypertension, and metabolic disorders [1–7]. Therefore, assessing noise exposure during this critical timeframe is essential for evaluating the true impact of urban mobility transitions, particularly the shift from ICEVs to EVs, and for informing noise mitigation strategies that prioritize public health.

4.1. Impact on long-term averages

As a first result, Fig. 5 presents the equivalent continuous night-time sound pressure level L_{Night} computed from the time-resolved noise maps for the period from 11 p.m. to 7 a.m. As expected, the highest noise levels are concentrated along the major traffic arteries, where L_{Night} reaches values up to 75 dB(A). However, noise levels decrease rapidly with increasing distance from the road, and values on the nearest building façades typically do not exceed 70 dB(A). These levels nonetheless represent a significant source of annoyance, and long-term exposure can substantially impact the quality of life for residents.

The lesser-frequented roads exhibit average night-time noise levels of around 60 dB(A), reflecting moderate traffic activity. Small residential streets, characterized by low traffic volumes and speed limits, typically show noise levels below 50 dB(A), creating a favorable acoustic environment for nighttime rest, likely leading to improved sleep quality and reduced annoyance.

Having established the night-time noise levels for a conventional fleet of ICEVs as a baseline scenario, we now investigate the acoustic consequences of transitioning to a modernized fleet dominated by EVs. To this end, all vehicles in category 1 (as defined in Section 2.4) are replaced with their electric counterparts, while preserving their kinematic behavior, i.e., their trajectories, speed, and acceleration patterns, ensuring a fair comparison based solely on noise emission characteristics. To model the noise emission of EVs, two recently proposed modifications of the CNOSSOS-EU emission coefficients are implemented and compared: the models of Pallas et al. [35] and Licitra et al. [36] (see Section 3).

As a first insight into the impact of transitioning from a conventional fleet of ICEVs to EVs, Fig. 6 presents the difference in equivalent continuous night-time sound pressure level, $\Delta L_{\mathrm{Night}} = L_{\mathrm{Night}}^{(\mathrm{ICEVs})} - L_{\mathrm{Night}}^{(\mathrm{EVs})}$, computed using the two distinct EV emission models. In subfigure (a) the model of Pallas et al. is employed, while the results shown in subfigure (b) are obtained using the model proposed by Licitra et al. In both cases, a clear trend emerges: the introduction of EVs leads to significant reductions in average noise levels along less-frequented residential roads, whereas the impact is considerably smaller along major traffic arteries. This pattern is primarily attributable to the dominance of rolling noise at speeds above 30 km/h,[2] where the difference in rolling noise emission from ICEVs and EVs never exceeds 2.9 dB(A) when using the Pallas et al. model, and is less than 5.2 dB(A) when the model of Licitra et al. is applied. Consequently, using the Pallas et al. model (Fig. 6a), noise reductions are limited to approximately 3 dB(A) along arterial roads with speed limits of 50 km/h, while the Licitra et al. model (Fig. 6b) predicts more pronounced reductions of around 5 dB(A).

On the low-speed residential streets the Pallas et al. and Licitra et al. models predict noise reductions of about 5 dB(A) and 8 dB(A), respectively. These results compare fairly well to the corresponding reductions in total noise emission at a speed of 30 km/h, which amount to 4.6 dB(A) and 7.4 dB(A) when comparing ICEVs to EVs using the two emission models. When averaged over the entire domain, the Pallas et al. model predicts an overall noise reduction of 3.8 dB(A), whereas the Licitra et al. model yields a higher average reduction of 4.7 dB(A).

Fig. 7 shows the difference in equivalent continuous night-time sound level, $\Delta L_{\mathrm{Night}} = L_{\mathrm{Night}}^{(\mathrm{EVs\ Pallas})} - L_{\mathrm{Night}}^{(\mathrm{EVs\ Licitra})}$, between the two EV emission models, enabling a more detailed comparison of their acoustic predictions. As previously noted in the context of Fig. 6, the Pallas et al. model predicts higher average noise levels across the vast majority of the domain, which albeit the lack of propulsion noise in the Licitra et al. framework, is primarily due to its more elevated rolling noise emissions. Specifically, the difference in rolling noise emission is 2.4 dB(A) at 30 km/h and 1.6 dB(A) at 50 km/h, which accounts for the majority of the observed differences in L_{Night}, which is approximately 3.0 dB(A) and 1.7 dB(A) along residential and major roads, respectively. The remaining discrepancy is attributed to the contribution of propulsion noise to the total emitted sound-power level L_W in the Pallas et al. model, which is 0.4 dB(A) at 30 km/h and 0.1 dB(A) at 50 km/h, and is neglected in the Licitra et al. framework.

[2] More precisely, rolling noise dominates ICEV noise emissions above 26 km/h. In contrast, the rolling noise component always dominates the emissions of EVs (See Fig. 3).

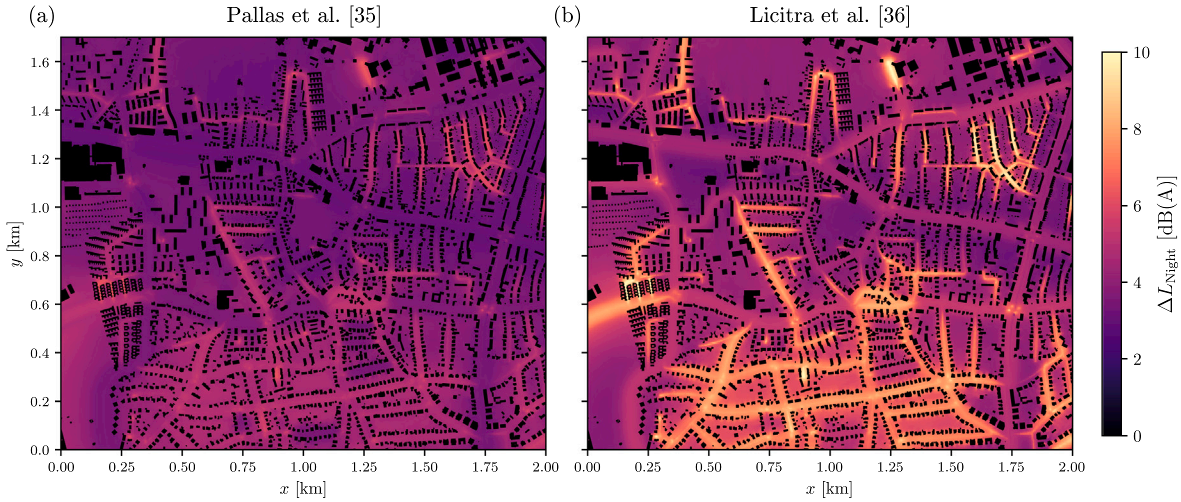

Fig. 6. Difference in equivalent continuous night-time sound pressure level, $\Delta L_{\text{Night}} = L_{\text{Night}}^{(\text{ICEVs})} - L_{\text{Night}}^{(\text{EVs})}$, obtained for a conventional ICEV fleet and a modernized fleet dominated by EVs. Subfigure (a) uses the EV emission model proposed by Pallas et al. [35], while subfigure (b) employs the model by Licitra et al. [36]. Both color maps use the scale indicated by the color bar on the right, which accounts for differences up to 10 dB(A). Black polygons represent buildings within the domain.

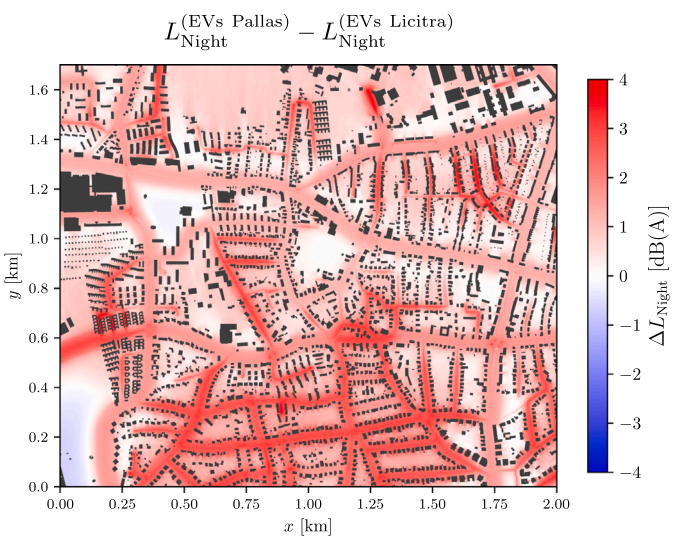

Fig. 7. Difference in equivalent continuous night-time sound pressure level, $\Delta L_{\text{Night}} = L_{\text{Night}}^{(\text{EVs Pallas})} - L_{\text{Night}}^{(\text{EVs Licitra})}$, obtained for a fleet dominated by EVs using the emission models proposed by Pallas et al. [35] and Licitra et al. [36]. The color map accounts for differences ranging from −4 to 4 dB(A), as indicated by the color bar on the right, and grey polygons represent buildings within the domain.

In the unobstructed far-field, where atmospheric absorption primarily attenuates higher frequencies, low-frequency components dominate. Only here, the Licitra et al. model predicts slightly higher noise levels than the Pallas et al. model [≈ 0.5 dB(A), see bottom-left corner of Fig. 7]. This is primarily due to the Licitra et al. model's higher rolling noise emissions in the low-frequency bands (63 to 500 Hz) at speeds below 80 km/h,[3] which become more prominent at greater distances from the sources.

Note that these conclusions are valid only for unobstructed far-field regions, where no diffracting obstacles lie between the sources and receivers, such as in the south-western part of the study domain (see Fig. 7). In contrast, the far-field areas to the north are separated from the road network by buildings, which cause significant sound diffraction and attenuation, particularly for low-frequency components. As a result, high-frequency components of rolling noise dominate in the northern far-field regions, where the Pallas et al. model predicts higher emissions. This explains the observed differences between the northern and south-western far-field regions as a consequence of the distinct spectral distributions of rolling noise in the two emission models.

4.2. Impact on wake-up reactions

To gain deeper insight into the impact of the transition from ICEVs to a modernized fleet dominated by EVs on sleep disturbances and associated human health implications, 14 representative locations have been selected within the domain (see Fig. 8a) to monitor individual vehicle pass-by events during the nighttime hours. This approach leverages the time-resolved nature of the noise maps, enabling a detailed analysis of the temporal characteristics of the noise caused by the pass-by events. Correlating these characteristics, particularly the maximum SPL $L_{\max}$, with an exposure-response relationship allows us to estimate the probability that the individual events trigger wake-up reactions in nearby residents.

At the 14 selected locations, highlighted in Fig. 8(a), a line crossing all lanes of the adjacent road is assumed. Vehicle trajectories are tracked to identify isolated pass-by events: a vehicle pass-by is considered isolated if no other vehicle crossed the line within 10 s before and after. At each location, a receiver point is placed 2 m in front of the nearest building façade at a height of 1.5 m, representing a ground-floor window facing the street. The direct (3D) distance d of these receiver points to the nearest lane of the road network varies between 4.1 m and 16.6 m for the 14 selected locations, as reported in Table 2. The time-resolved SPL at the individual receiver locations is monitored during each pass-by event to assess the noise exposure of a resident assumed to be sleeping indoors. Notice that our assumptions reflect a worst-case scenario: individuals sleeping in a ground-floor room directly adjacent to the road. The following analysis thus focuses on this high-exposure group, who are most affected by nighttime traffic noise.

As an example, Fig. 8(b) shows the time-resolved outdoor SPL for a time window surrounding the $N = 122$ isolated pass-by events detected at location 9 for the case of a conventional ICEV fleet. As expected, each curve exhibits a sharp, isolated peak at the time t_0 when the

[3] Although the Licitra et al. model predicts higher low-frequency rolling noise emissions, the total energetic sum across all bands always remains lower than in the Pallas et al. model (see Fig. 3).

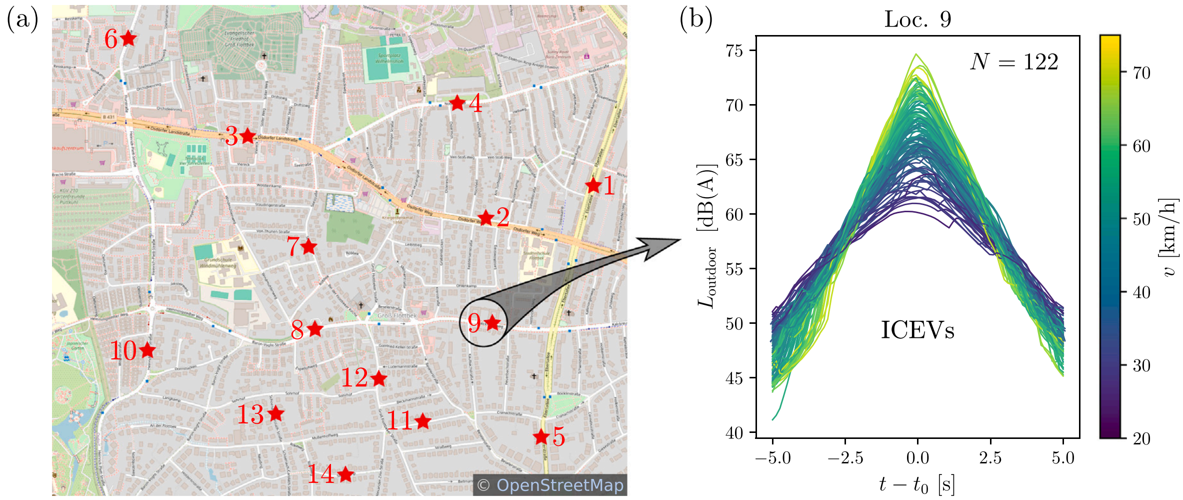

Fig. 8. (a) Selected locations for monitoring individual vehicle pass-by events during the nighttime. The underlying map is taken from OpenStreetMap (©OpenStreetMap contributors [40]). (b) Time-resolved outdoor SPL for the $N = 122$ isolated pass-by events detected at location 9. Each curve is centered at the time t_0 when the vehicle pass-by is detected and is color-coded according to the vehicle's speed, as indicated by the color bar on the right.

Table 2
Statistical estimates for wake-up reactions induced by night-time traffic noise at 14 selected probe locations. Provided is the total number N of isolated pass-by events during the night, the Direct (3D) distance d from the probe location to the nearest road lane, the expected number of induced wake-up reactions $\langle N_w \rangle = \sum_{n=1}^{N} p_n$ along with its standard deviation $\sigma_{N_w} = \sqrt{\sum_{n=1}^{N} p_n (1 - p_n)}$, and the probability of awakening at least Once during the night $P_1 = 1 - \prod_{n=1}^{N}(1 - p_n)$. Here $p_n = p_w\left(L_{\max}^{(n)}\right)$ is the wake-up probability for the n-th pass-by event and the exposure-response relation of Sanok et al. [34] is applied to map the maximum indoor SPL $L_{\max}$ to the wake-up probability p_w. Additionally, for ICEVs the equivalent continuous night-time sound level L_{Night} at the 14 probe locations is provided, while for EVs the corresponding reduction $\Delta L_{\mathrm{Night}} = L_{\mathrm{Night}}^{(\mathrm{ICEVs})} - L_{\mathrm{Night}}^{(\mathrm{EVs})}$ is given.

			ICEVs				EVs (Pallas et al. [35])				EVs (Licitra et al. [36])			
Loc.	N	d [m]	L [dBA]	$\langle N_w \rangle$	σ_{N_w}	P_1	ΔL [dBA]	$\langle N_w \rangle$	σ_{N_w}	P_1	ΔL [dBA]	$\langle N_w \rangle$	σ_{N_w}	P_1
1	402	6.2	60.9	3.66	1.90	97.5%	3.05	2.97	1.71	94.9%	4.24	2.67	1.63	93.1%
2	310	7.9	61.9	2.17	1.47	88.7%	3.11	1.68	1.29	81.5%	4.33	1.46	1.21	76.9%
3	298	4.1	67.2	3.36	1.82	96.6%	3.21	2.77	1.65	93.8%	4.57	2.49	1.57	91.8%
4	171	7.1	54.5	1.82	1.34	84.0%	3.50	1.49	1.21	77.6%	5.04	1.34	1.15	74.0%
5	171	11.8	52.6	1.60	1.26	80.0%	3.48	1.29	1.13	72.6%	4.97	1.15	1.07	68.5%
6	156	9.3	54.6	1.53	1.23	78.5%	3.39	1.24	1.11	71.1%	4.86	1.10	1.05	66.9%
7	145	14.2	47.3	0.86	0.93	58.0%	3.18	0.59	0.76	44.5%	4.35	0.45	0.67	36.2%
8	125	5.1	53.8	1.42	1.19	76.1%	3.66	1.17	1.07	69.0%	5.35	1.04	1.02	65.0%
9	122	11.1	51.7	1.06	1.02	65.4%	3.64	0.84	0.91	56.8%	5.29	0.74	0.86	52.4%
10	113	16.6	48.0	0.87	0.93	58.2%	3.55	0.68	0.82	49.5%	5.06	0.60	0.77	45.1%
11	35	9.7	40.9	0.23	0.48	20.9%	4.92	0.16	0.40	14.7%	7.64	0.12	0.35	11.4%
12	20	11.8	39.1	0.13	0.36	12.2%	4.59	0.09	0.30	8.71%	7.13	0.07	0.27	6.87%
13	8	10.5	34.4	0.05	0.23	5.18%	4.65	0.04	0.19	3.62%	7.12	0.03	0.17	2.83%
14	4	8.4	35.2	0.04	0.19	3.75%	3.58	0.03	0.17	3.02%	5.21	0.03	0.16	2.68%

vehicle crosses the monitoring line. With increasing vehicle speed v, the maximum sound pressure level $L_{\max}$ rises, and the peak becomes narrower. The increase in $L_{\max}$ is directly correlated with the higher sound-power emission at higher speeds, while the peak narrowing results from the reduced time a faster vehicle spends in the vicinity of the receiver, leading to a shorter exposure duration.

To estimate the indoor SPL caused by an individual pass-by event, 15.8 dB is subtracted from the time-resolved outdoor SPL, a value that represents the typical difference between indoor and outdoor sound levels if the bedroom window is assumed to be tilted, as reported by Locher et al. [47]. Using this indoor SPL estimate, the exposure-response relationship established by Sanok et al. [34] is applied, which links the maximum sound pressure level $L_{\max}$ at the ear of a sleeping resident caused by a single vehicle pass-by to the probability $p_w(L_{\max})$ that a wake-up reaction is triggered. Using this model, one readily obtains the expected number of wake-up reactions during the night, $\langle N_w \rangle = \sum_n p_n$, along with its standard deviation, $\sigma_{N_w} = \sqrt{\sum_n p_n (1 - p_n)}$, and the probability of awakening at least once during the night, $P_1 = 1 - \prod_n (1 - p_n)$, where $p_n = p_w\left(L_{\max}^{(n)}\right)$ is the wake-up probability for the n-th pass-by event. These quantities are summarized in Table 2 for the 14 selected locations, under both a conventional ICEV fleet and a modernized fleet dominated by EVs, using the emission models of Pallas et al. [35] and Licitra et al. [36]. To enable a direct comparison with the average night-time noise levels presented in Section 4.1, Table 2 also reports L_{Night} at each of the 14 selected locations for the conventional ICEV fleet, along with the corresponding difference $\Delta L_{\mathrm{Night}} = L_{\mathrm{Night}}^{(\mathrm{ICEVs})} - L_{\mathrm{Night}}^{(\mathrm{EVs})}$ obtained for a modernized EV fleet.

Averaging across all 14 probe locations, a conventional ICEV fleet causes an average of 1.34 wake-up reactions per night. For a modernized EV fleet, the Pallas et al. model predicts a reduction to 1.07, while the Licitra et al. model yields an even lower average of 0.95 wake-up reactions. Correspondingly, the probability of at least one wake-up event during the night decreases from an average of 58.9% under ICEVs to 53.0% and 49.5% for the Pallas et al. and Licitra et al. models, respectively. Although the reduction in wake-up probability is rather moderate, it demonstrates that the transition to EVs offers tangible benefits beyond environmental goals, improving sleep quality and reducing noise-related health risks for urban residents.

The greatest impact on the expected number of wake-up reactions is observed along major arterial roads (locations 1–5) with speed limits of 50 km/h, where ICEVs lead to an average of 2.5 wake-up events per night. Under the EV fleet, this value drops to 2.0 (Pallas et al. model) and 1.8 (Licitra et al.), with the probability of at least one awakening decreasing from 89.3% to 84.1% and 80.9%, respectively. These reductions on major roads are accompanied by an average decrease of L_{Night} by 3.27 dB(A) (Pallas et al. model) and 4.63 dB(A) (Licitra et al. model).

On intermediate-traffic roads (locations 6–10), having speed limits of 50 km/h except for location 7, where the speed limit is 30 km/h, the average number of wake-up reactions decreases from 1.15 (ICEVs) to 0.90 (Pallas et al.) and 0.79 (Licitra et al.). Along these intermediate-traffic roads the greatest decrease in the probability of experiencing at least one awakening during the night is observed, which drops from 67.2% (ICEVs) to 58.2% (Pallas et al.) and 53.1% (Licitra et al.). The corresponding drop in L_{Night} is 3.48 dB(A) (Pallas et al.) and 4.98 dB(A) (Licitra et al.), respectively.

Finally, on residential streets (locations 11–14), where traffic is light and speed limits are 30 km/h, the baseline average wake-up risk is already low: $\langle N_w \rangle = 0.11$ and $P_1 = 10.5\%$ for ICEVs. EV adoption further reduces these values slightly: $\langle N_w \rangle = 0.08$ ($P_1 = 7.5\%$) and $\langle N_w \rangle = 0.06$ ($P_1 = 5.9\%$) for the Pallas et al. and Licitra et al. models, respectively. The associated L_{Night} reductions are, however, substantial: 4.44 dB(A) (Pallas et al.) and 6.78 dB(A) (Licitra et al.).

5. Discussion

The results presented in Section 4.2 indicate that the impact of EV adoption on sleep quality is moderate overall. The greatest reduction in the expected number of induced wake-up reactions $\langle N_w \rangle$ during the night occurs in the vicinity of major traffic arteries (locations 1–5), where the simulations using the Licitra et al. model predict an average reduction of 0.7, while a reduction of 0.5 is obtained in the framework of the Pallas et al. model. Smaller reductions in $\langle N_w \rangle$ are observed in the vicinity of intermediate-traffic and residential roads.

Regarding the probability P_1 of awakening at least once during the nighttime, both models predict the greatest impact from EV adoption in the vicinity of intermediate-traffic roads. Averaged over all intermediate-traffic locations (6–10), P_1 decreases by 14.1% and 9.0% using the Licitra et al. and Pallas et al. models, respectively.

These findings are in contrast with the predictions derived from the averaged noise maps in Section 4.1, which show the largest reduction of L_{Night} in the vicinity of small residential roads. Here the baseline wake-up risk is already low under the conventional ICEV fleet, and the reduction in $\langle N_w \rangle$ by 0.05 (0.03) and P_1 by 4.6% (3%) due to EV adoption predicted by the Licitra et al. (Pallas et al.) model is rather small compared to the effects observed on major and intermediate-traffic roads. This dissociation highlights the limitations of relying solely on long-term averages like L_{Night} for assessing the health impact of traffic noise. Instead, time-resolved noise mapping techniques, though computationally more demanding, enable the analysis of transient events and their physiological effects and are thus essential for a comprehensive evaluation of noise exposure.

Comparing the two EV emission models, the one by Licitra et al. predicts lower noise levels of EVs across the vast majority of the domain, which is most likely attributable to its foundation in noise measurements of more modern EVs, reflecting the technological progress in noise reduction over several years. As such, it is considered more representative of current and future EV fleets. Although propulsion noise is neglected entirely in the Licitra et al. model, the key difference between the two models is found to be their treatment of rolling noise: while the Pallas et al. model relies on the CNOSSOS-EU rolling noise model for category 1 vehicles, the Licitra et al. model provides optimized emission coefficients specifically tailored to model the rolling-noise emissions of modern EVs. It is worth noting that neither of the EV emission models considered in this study includes the acoustic output of an Acoustic Vehicle Alerting System (AVAS), which is now mandatory for new electric and hybrid vehicles to alert vulnerable road users. Given its potential impact, particularly in low-traffic residential areas, incorporating AVAS into updated EV emission models is important for future developments.

The present results are obtained on the basis of several key assumptions and simplifications, which are briefly revisited and discussed in the following in order to allow for a transparent and comprehensive interpretation.

- For sound propagation modeling, the terrain is assumed to be flat and vegetation is neglected. Building geometries are represented at LoD1, capturing only the basic footprint and height of structures.
- Reference conditions are assumed for the noise emission: an air temperature of 20 °C and a dry road surface consisting of dense asphalt concrete. Furthermore, a semi-custom correction for the acceleration noise, defined by Eqs. (4) and (5), is applied to both ICEVs and EVs. Future studies may refine this approach by incorporating dedicated correction models for EVs, such as the one proposed by Baclet et al. [45].
- The transition from ICEVs to EVs is modeled by assuming that all vehicles in category 1 (light motor vehicles) are replaced by their electric counterparts. Vehicles in categories 2–4 are assumed to remain conventional ICEVs. Future studies may extend this approach by incorporating EV emission models for categories 2–4 and by using realistic distributions of ICEVs and EVs within each category.
- To estimate the impact on wake-up reactions, a resident sleeping in a ground-floor room with a window facing the street is assumed. This represents the most vulnerable group, which is most exposed to nighttime traffic noise. Furthermore, the difference between outdoor and indoor sound levels is estimated at 15.8 dB, a commonly used value for the sound insulation of a typical building façade when the bedroom window is tilted [47]. However, actual values depend strongly on the building construction, window type, and occupant behavior (sleeping with an open, tilted or closed window).
- To link the maximum sound-pressure level $L_{\max}$ caused by individual vehicle pass-by events to the corresponding probability of inducing a wake-up reaction, the exposure-response relationship derived by Sanok et al. [34] is employed. This model represents an average across the forty healthy participants of the field study conducted by Sanok et al., and thus reflects population-level responses rather than individual variability. As wake-up probability varies significantly among individuals, the present results should be interpreted as predictions for the average resident, not for specific individuals.
- The study domain was selected to provide a representative mix of high-traffic arterial roads, intermediate-traffic roads, and smaller residential streets. As such, the results are representative of typical urban environments in Europe, particularly in Germany.

6. Conclusion

This study presents a time-resolved noise mapping framework which is based on the provisions of the CNOSSOS-EU guideline. It is applied to assess the acoustic impact of transitioning from internal combustion engine vehicles (ICEVs) to electric vehicles (EVs) in urban environments. The method relies on the microscopic traffic simulation SUMO [37], which provides time-resolved trajectories of individual vehicles. This enables the detailed analysis of transient traffic noise events which are key drivers of human perception and physiological responses such as sleep disturbance.

The study area is the district Gross Flottbek in Hamburg, Germany, which offers a representative mix of quieter residential streets and high-traffic arterial roads, making it well-suited for evaluating the acoustic effects of fleet electrification across diverse urban scenarios.

To evaluate the implications of the transition from conventional ICEVs to a modernized fleet dominated by EVs, time-resolved noise maps are generated covering the selected region. Two recently proposed EV emission models by Pallas et al. [35] and Licitra et al. [36] are applied to predict noise levels of an EV fleet. Regarding the equivalent continuous night-time sound level L_{Night}, the Pallas et al. model predicts reductions of approximately 3 dB(A) along major arterial roads and 5 dB(A) near residential roads. The Licitra et al. model yields higher reductions: about 5 dB(A) on major roads and up to 8 dB(A) in residential areas.

Leveraging the time-resolved nature of the noise maps, individual vehicle pass-by events are monitored during the nighttime at 14 representative probe locations, enabling the detailed assessment of transient noise patterns. The exposure-response relationship established by Sanok et al. [34], which links the maximum indoor sound-pressure level (SPL) $L_{\max}$ of an isolated vehicle pass-by event to the wake-up probability p_w, is applied to estimate the impact on sleep quality caused by the transition from ICEVs to a modern EVs fleet.

Our findings indicate that the overall impact on sleep quality from the transition to a fleet dominated by EVs remains moderate: In the vicinity of a typical intermediate-traffic road, the probability of awakening during the night decreases by about 14%, with smaller reductions on major and residential roads. The expected number of wake-up reactions per night decreases by about 0.7 for residents living near major traffic arteries, with smaller reductions in the areas of intermediate-traffic and small residential roads. These findings are in contrast to the trends observed in L_{Night}, which predict the most significant reductions in residential areas. This divergence highlights the limitations of relying solely on average noise metrics and underscores the need for complementary, event-based indicators capable of capturing the temporal dynamics of traffic noise.

CRediT authorship contribution statement

Tobias S. Müller: Writing – review & editing, Writing – original draft, Visualization, Software, Methodology, Investigation, Formal analysis, Data curation, Conceptualization. **Daniel Krajzewicz:** Validation, Resources, Investigation, Data curation. **Arne Henning:** Supervision, Project administration, Funding acquisition, Conceptualization.

Declaration of Generative AI and AI-assisted technologies in the writing process

During the preparation of this work the authors used AI-assisted writing and editing tools (Qwen 3 30B A3B Instruct 2507, developed by Alibaba Cloud) in order to support the refinement of scientific language, improve sentence structure, and assist with spelling and grammar. After using this tool, the authors reviewed and edited the content as needed and take full responsibility for the content of the published article.

Declaration of competing interest

The authors declare that they have no known competing financial interests or personal relationships that could have appeared to influence the work reported in this paper.

Acknowledgements

The authors gratefully acknowledge the scientific support and HPC resources provided by the German Aerospace Center (DLR). The HPC system CARO is partially funded by “Ministry of Science and Culture of Lower Saxony” and “Federal Ministry for Economic Affairs and Climate Action”.

Data availability

The authors do not have permission to share data.

References

[1] European Environment Agency. Healthy environment, healthy lives: how the environment influences health and well-being in Europe. EEA Report NO 21/2019 Luxembourg: Publications Office of the European Union 2020.

[2] Griefahn B, Marks A, Robens S. Noise emitted from road, rail and air traffic and their effects on sleep. J Sound Vib 2006;295:129–40. https://doi.org/10.1016/j.jsv.2005.12.052

[3] Muzet A. Environmental noise, sleep and health. Sleep Med Rev 2007;11:135–42. https://doi.org/10.1016/j.smrv.2006.09.001

[4] Pirrera S, De Valck E, Cluydts R. Nocturnal road traffic noise: a review on its assessment and consequences on sleep and health. Environ Int 2010;36:492–8. https://doi.org/10.1016/j.envint.2010.03.007

[5] Aasvang GM, Øverland B, Ursin R, Moum T. A field study of effects of road traffic and railway noise on polysomnographic sleep parameters. J Acoust Soc Am 2011;129:3716–26. https://doi.org/10.1121/1.3583547

[6] Clark C, Crumpler C, Notley H. Evidence for environmental noise effects on health for the United Kingdom policy context: a systematic review of the effects of environmental noise on mental health, wellbeing, quality of life, cancer, dementia, birth, reproductive outcomes, and cognition. Int J Environ Res Public Health 2020;17:393. https://doi.org/10.3390/ijerph17020393

[7] Fu X, Wang L, Yuan L, Hu H, Li T, Zhang J, Ke Y, Wang M, Gao Y, Huo W, Chen Y, Zhang W, Liu J, Huang Z, Zhao Y, Hu F, Zhang M, Liu Y, Sun X, Hu D. Long-term exposure to traffic noise and risk of incident cardiovascular diseases: a systematic review and dose-response meta-analysis. J Urban Health 2023;100:788–801. https://doi.org/10.1007/s11524-023-00769-0

[8] Fritschi L, Brown AL, Kim R, Schwela D, Kephalopoulos S. Burden of disease from environmental noise. Bonn: World Health Organization; 2011.

[9] European Union. Directive 2002/49/EC of the European parliament and of the council of 25 June 2002 relating to the assessment and management of environmental noise. Off J L 2002;189, 18.7.2002, p. 12.

[10] Kephalopoulos S, Paviotti M, Anfosso-Lédée F. Common noise assessment methods in Europe (CNOSSOS-EU). Scientific and Technical Report EUR 25379 EN Luxembourg: Publications Office of the European Union; 2012. https://doi.org/10.2788/32029

[11] Campello-Vicente H, Peral-Orts R, Campillo-Davo N, Velasco-Sanchez E. The effect of electric vehicles on urban noise maps. Appl Acoust 2017;116:59–64. https://doi.org/10.1016/j.apacoust.2016.09.018

[12] Yang W, He J, He C, Cai M. Evaluation of urban traffic noise pollution based on noise maps. Transp Res D Transp Environ 2020;87:102516. https://doi.org/10.1016/j.trd.2020.102516

[13] Le Bescond V, Can A, Aumond P, Gastineau P. Open-source modeling chain for the dynamic assessment of road traffic noise exposure. Transp Res D Transp Environ 2021;94:102793. https://doi.org/10.1016/j.trd.2021.102793

[14] Baclet S, Nygren J, Rumpler R. Impact of car electrification on urban noise pollution: a microscopic traffic simulation study. In: INTER-NOISE and NOISE-CON congress and conference proceedings, vol. 270; 2024. p. 7846–55. https://doi.org/10.3397/in_2024_4014

[15] Baclet S, Venkataraman S, Rumpler R, Billsjö R, Horvath J, Österlund PE. From strategic noise maps to receiver-centric noise exposure sensitivity mapping. Transp Res D Transp Environ 2022;102:103114. https://doi.org/10.1016/j.trd.2021.103114

[16] Baffoe PE, Duker AA, Senkyire-Kwarteng EV. Assessment of health impacts of noise pollution in the Tarkwa mining community of Ghana using noise mapping techniques. Glob Health J 2022;6:19–29. https://doi.org/10.1016/j.glohj.2022.01.005

[17] Khomenko S, Cirach M, Barrera-Gómez J, Pereira-Barboza E, Iungman T, Mueller N, Foraster M, Tonne C, Thondoo M, Jephcote C, Gulliver J, Woodcock J, Nieuwenhuijsen M. Impact of road traffic noise on annoyance and preventable mortality in European cities: a health impact assessment. Environ Int 2022;162:107160. https://doi.org/10.1016/j.envint.2022.107160

[18] Murphy E, King E. Environmental noise pollution: noise mapping, public health, and policy. Elsevier; 2022.

[19] Smith MG, Cordoza M, Basner M. Environmental noise and effects on sleep: an update to the WHO systematic review and meta-analysis. Environ Health Perspect 2022;130. https://doi.org/10.1289/ehp10197

[20] Wei W, Van Renterghem T, De Coensel B, Botteldooren D. Dynamic noise mapping: a map-based interpolation between noise measurements with high temporal resolution. Appl Acoust 2016;101:127–40. https://doi.org/10.1016/j.apacoust.2015.08.005

[21] Sevillano X, Socoró JC, Alías F, Bellucci P, Peruzzi L, Radaelli S, Coppi P, Nencini L, Cerniglia A, Bisceglie A, Benocci R, Zambon G. DYNAMAP – development of low cost sensors networks for real time noise mapping. Noise Mapp 2016;3:172–89. https://doi.org/10.1515/noise-2016-0013

[22] Aumond P, Can A, Mallet V, De Coensel B, Ribeiro C, Botteldooren D, Lavandier C. Kriging-based spatial interpolation from measurements for sound level mapping in urban areas. J Acoust Soc Am 2018;143:2847–57. https://doi.org/10.1121/1.5034799

[23] Chevallier E, Can A, Nadji M, Leclercq L. Improving noise assessment at intersections by modeling traffic dynamics. Transp Res D Transp Environ 2009;14:100–10. https://doi.org/10.1016/j.trd.2008.09.014

[24] Cucurachi S, Schiess S, Froemelt A, Hellweg S. Noise footprint from personal land-based mobility. J Ind Ecol 2019;23:1028–38. https://doi.org/10.1111/jiec.12837

[25] Zwick F, Kuehnel N, Moeckel R, Axhausen KW. Agent-based simulation of city-wide autonomous ride-pooling and the impact on traffic noise. Transp Res D Transp Environ 2021;90:102673. https://doi.org/10.1016/j.trd.2020.102673

[26] Xia-Lin M, Ming C. Rendering of dynamic road traffic noise map based on paramics. Procedia - Soc Behav Sci 2013;96:1460–8. https://doi.org/10.1016/j.sbspro.2013.08.166

[27] Baclet S, Khoshkhah K, Pourmoradnasseri M, Rumpler R, Hadachi A. Near-real-time dynamic noise mapping and exposure assessment using calibrated microscopic traffic simulations. Transp Res D Transp Environ 2023;124:103922. https://doi.org/10.1016/j.trd.2023.103922

[28] Li F, Lai R, Rong Y, Yu F, Du C, Lan Z, Ye B, Li Z. Dynamic traffic noise simulation at signal-controlled intersections based on cellular automata model. Appl Acoust 2024;224:110128. https://doi.org/10.1016/j.apacoust.2024.110128

[29] Wang H, Wu Z, Chen J. A prediction method for city traffic noise based on traffic simulation under a mixed distribution probability. Sustainability 2024;16:7065. https://doi.org/10.3390/su16167065

[30] Eberhardt J, Stråle L-O, Berlin M. The influence of continuous and intermittent traffic noise on sleep. J Sound Vib 1987;116:445–64. https://doi.org/10.1016/s0022-460x(87)81376-7

[31] Öhrström E, Rylander R, Björkman M. Effects of night time road traffic noise—an overview of laboratory and field studies on noise dose and subjective noise sensitivity. J Sound Vib 1988;127:441–8. https://doi.org/10.1016/0022-460x(88)90368-9

[32] Marks A, Griefahn B, Basner M. Event-related awakenings caused by nocturnal transportation noise. Noise Control Eng J 2008;56:52. https://doi.org/10.3397/1.2828211

[33] Wunderli JM, Pieren R, Habermacher M, Vienneau D, Cajochen C, Probst-Hensch N, Röösli M, Brink M. Intermittency ratio: a metric reflecting short-term temporal variations of transportation noise exposure. J Expo Sci Environ Epidemiol 2015;26:575–85. https://doi.org/10.1038/jes.2015.56

[34] Sanok S, Berger M, Müller U, Schmid M, Weidenfeld S, Elmenhorst E-M, Aeschbach D. Road traffic noise impacts sleep continuity in suburban residents: exposure-response quantification of noise-induced awakenings from vehicle pass-bys at night. Sci Total Environ 2022;817:152594. https://doi.org/10.1016/j.scitotenv.2021.152594

[35] Pallas M-A, Bérengier M, Chatagnon R, Czuka M, Conter M, Muirhead M. Towards a model for electric vehicle noise emission in the European prediction method CNOSSOS-EU. Appl Acoust 2016;113:89–101. https://doi.org/10.1016/j.apacoust.2016.06.012

[36] Licitra G, Bernardini M, Moreno R, Bianco F, Fredianelli L. CNOSSOS-EU coefficients for electric vehicle noise emission. Appl Acoust 2023;211:109511. https://doi.org/10.1016/j.apacoust.2023.109511

[37] Lopez PA, Behrisch M, Bieker-Walz L, Erdmann J, Flötteröd Y-P, Hilbrich R, Lücken L, Rummel J, Wagner P, Wiessner E. Microscopic traffic simulation using SUMO. In: 2018 21st international conference on intelligent transportation systems (ITSC); 2018. p. 2575–82. https://doi.org/10.1109/ITSC.2018.8569938

[38] Heinrichs M, Krajzewicz D, Cyganski R, von Schmidt A. Disaggregated car Fleets in microscopic travel demand modelling. Procedia Comput Sci 2016;83:155–62. https://doi.org/10.1016/j.procs.2016.04.111

[39] Schrader M, Karnik A, Hainen A, Bittle J. Calibrating car-following models using SUMO-in-the-loop and vehicle trajectories from roadside radar: calibrating CF model parameters. In: SUMO conference proceedings, vol. 5; 2024. p. 209–33. https://doi.org/10.52825/scp.v5i.1127

[40] OpenStreetMap contributors. Planet dump retrieved from https://planet.osm.org; 2017. https://www.openstreetmap.org.

[41] Borish J. Extension of the image model to arbitrary polyhedra. J Acoust Soc Am 1984;75:1827–36. https://doi.org/10.1121/1.390983

[42] Lee H, Lee B-H. An efficient algorithm for the image model technique. Appl Acoust 1988;24:87–115. https://doi.org/10.1016/0003-682x(88)90033-3

[43] Bundesministerium der Justiz und für Verbraucherschutz. Berechnungsmethode für den Umgebungslärm von bodennahen Quellen (Straßen, Schienenwege, Industrie und Gewerbe) (BUB). Bundesanzeiger (BAnz) AT 05.10.2021 B4. 2021.

[44] European Union. Commission delegated directive (EU) 2021/1226 of 21 December 2020 amending, for the purposes of adapting to scientific and technical progress, Annex II to directive 2002/49/EC of the European parliament and of the council as regards common noise assessment methods. Official Journal L 269, 28.7.2021, pp. 65–142 2021.

[45] Baclet S, Cesbron J, Aumond P, Can A, Rumpler R. A correction model for the noise emissions of light electric vehicles during acceleration. Appl Acoust 2025;236:110713. https://doi.org/10.1016/j.apacoust.2025.110713

[46] Pallas M-A. Comments on "CNOSSOS-EU coefficients for electric vehicle noise emission" [Appl. Acoust. 211 (2023) 109511] by G. licitra et al. Appl Acoust 2024;218:109871. https://doi.org/10.1016/j.apacoust.2024.109871

[47] Locher B, Piquerez A, Habermacher M, Ragettli M, Röösli M, Brink M, Cajochen C, Vienneau D, Foraster M, Müller U, Wunderli J. Differences between outdoor and indoor sound levels for open, tilted, and closed windows. Int J Environ Res Public Health 2018;15:149. https://doi.org/10.3390/ijerph15010149